Received: 7 May 2018 | Revised: 1 October 2018 | Accepted: 2 October 2018

DOI: 10.1002/hbm.24429

WILEY

RESEARCH ARTICLE

Comparison of EEG microstates with resting state fMRI and FDG-PET measures in the default mode network via simultaneously recorded trimodal (PET/MR/EEG) data

Ravichandran Rajkumar[1,2,3] | Ezequiel Farrher[1] | Jörg Mauler[1] | Praveen Sripad[1] | Cláudia Régio Brambilla[1,2,3] | Elena Rota Kops[1] | Jürgen Scheins[1] | Jürgen Dammers[1] | Christoph Lerche[1] | Karl-Josef Langen[1,4] | Hans Herzog[1] | Bharat Biswal[5] | N. Jon Shah[1,3,6,7,8] | Irene Neuner[1,2,3]

[1]Institute of Neuroscience and Medicine 4, INM-4, Forschungszentrum Jülich, Jülich, Germany

[2]Department of Psychiatry, Psychotherapy and Psychosomatics, RWTH Aachen University, Aachen, Germany

[3]JARA – BRAIN – Translational Medicine, Aachen, Germany

[4]Department of Nuclear Medicine, RWTH Aachen University, Aachen, Germany

[5]Department of Biomedical Engineering, New Jersey Institute of Technology, Newark, New Jersey

[6]Institute of Neuroscience and Medicine 11, INM-11, Forschungszentrum Jülich, Jülich, Germany

[7]Department of Neurology, RWTH Aachen University, Aachen, Germany

[8]Monash Biomedical Imaging, School of Psychological Sciences, Monash University, Melbourne, Victoria, Australia

Correspondence
Irene Neuner, Institute of Neuroscience and Medicine 4, INM-4, Forschungszentrum Jülich GmbH, 52425 Jülich, Germany.
Email: i.neuner@fz-juelich.de

Funding information
Seventh Framework Programme, Grant/Award Number: 602621

Abstract

Simultaneous trimodal positron emission tomography/magnetic resonance imaging/electroencephalography (PET/MRI/EEG) resting state (rs) brain data were acquired from 10 healthy male volunteers. The rs-functional MRI (fMRI) metrics, such as regional homogeneity (ReHo), degree centrality (DC) and fractional amplitude of low-frequency fluctuations (fALFFs), as well as 2-[18F]fluoro-2-desoxy-D-glucose (FDG)-PET standardised uptake value (SUV), were calculated and the measures were extracted from the default mode network (DMN) regions of the brain. Similarly, four microstates for each subject, showing the diverse functional states of the whole brain via topographical variations due to global field power (GFP), were estimated from artefact-corrected EEG signals. In this exploratory analysis, the GFP of microstates was nonparametrically compared to rs-fMRI metrics and FDG-PET SUV measured in the DMN of the brain. The rs-fMRI metrics (ReHO, fALFF) and FDG-PET SUV did not show any significant correlations with any of the microstates. The DC metric showed a significant positive correlation with microstate C (r_s = 0.73, p = .01). FDG-PET SUVs indicate a trend for a negative correlation with microstates A, B and C. The positive correlation of microstate C with DC metrics suggests a functional relationship between cortical hubs in the frontal and occipital lobes. The results of this study suggest further exploration of this method in a larger sample and in patients with neuropsychiatric disorders. The aim of this exploratory pilot study is to lay the foundation for the development of such multimodal measures to be applied as biomarkers for diagnosis, disease staging, treatment response and monitoring of neuropsychiatric disorders.

KEYWORDS

18F-FDG, biomarkers, electroencephalography, fMRI, multimodal imaging, positron emission tomography

1 | INTRODUCTION

Recent developments in medical imaging technologies have made the simultaneous measurement of the three modalities, magnetic resonance imaging (MRI), positron emission tomography (PET) and electroencephalography (EEG), feasible (Shah et al., 2017). The main advantage of such technology is that structural and functional (via MRI), metabolic (via PET) and electrophysiological (via EEG) signatures can be confined simultaneously under the same physiological and psychological conditions (Shah et al., 2013). Exploitation of such simultaneous multimodal neuroimaging technology has enabled neuroscientists to explore the functioning of the human brain using the diverse information provided by each modality with different temporal and spatial resolutions. The complementary value of the

information provided by each modality is considerably increased by the simultaneous execution of MR, PET and EEG. The physiological information provided by each modality is as follows:

- Functional MRI (fMRI) measures brain activity in an indirect fashion via the blood oxygenation level-dependent (BOLD) contrast (Ogawa, Lee, Kay, & Tank, 1990).
- PET provides quantitative molecular information (Tomasi, Wang, & Volkow, 2013).
- EEG, a direct measure of neuronal activity records the electrophysiological signals of the brain with high temporal resolution. Electrical activity that occurs at synapses of neurons and changes in neuronal cell membrane permeability create EEG signals (Davidson, Jackson, & Larson, 2000).

A number of image and signal analysis methods (Abreu, Leal, & Figueiredo, 2018; Bai, Xia, & Li, 2017; Boellaard, 2008; Bowman, Guo, & Derado, 2007) are available to process, either qualitatively or quantitatively, the data obtained from each imaging modality. Combined analysis of the complimentary information provided by each modality can help in understanding the complex relationships between the various physiological mechanisms of the brain. The relationship between simultaneously recorded bimodalities, such as fMRI/PET (Aiello et al., 2015; Riedl et al., 2014, 2015), fMRI/EEG (Goldman, Stern, Engel, & Cohen, 2000; Huster, Debener, Eichele, & Herrmann, 2012; Ritter & Villringer, 2006) and PET/EEG (Hur, Lee, Lee, Yun, & Kim, 2013), has already been reported by a number of groups. Furthermore, other research has shown the feasibility and application (Golkowski et al., 2017; Del Guerra et al., 2017; Shah et al., 2017) of simultaneous trimodal (MR/PET/EEG) measurements. Even though various functional relationships between simultaneously recorded bimodal and trimodal data have already been investigated and reported on, an exploratory analysis on the neuroelectric (electrophysiology as measured by EEG) metrics and its relationship with neurovascular (hemodynamic response as measured by BOLD fMRI) and neurometabolic (metabolic activity as measured by PET) metrics on a simultaneously recorded resting state (rs) trimodal data set has not yet been reported. In this work, we performed an exploratory analysis on simultaneously recorded rs-trimodal data in order to elucidate the relationship between neuroelectric measures with neurovascular and neurometabolic measures.

Analysis of simultaneously recorded trimodal data can advance the understanding of the brain functions in general. The main future advantage of multimodal analysis techniques lies in the definition of image-based biomarkers for neurological and psychiatric disorders with the help of machine learning approaches (Polikar, Tilley, Hillis, & Clark, 2010). The simultaneous approach is especially valuable for the prediction of response to a given medication based on a pharmacological challenge during trimodal scanning (Bayouth et al., 2011). This would also prevent cofounding effects inevitable with separate scanning sessions (Laruelle et al., 1997). Also, by utilising the multimodal data, the accuracy in early diagnosis of neurological and psychiatric disorders could be improved. Furthermore, possibilities with regard to the potential applications of multimodal neuroimaging are already well reviewed and discussed in literature (Liu et al., 2015; O'Halloran, Kopell, Sprooten, Goodman, & Frangou, 2016; Uludağ & Roebroeck, 2014). A study has shown potential in vivo markers for neocortical neuronal loss in Alzheimer's disease by utilising multimodal evidence from MRI, PET and EEG (Hampel et al., 2002). A recently published pilot study has shown the feasibility of simultaneous trimodal data acquisition in schizophrenic patients (Del Guerra et al., 2017). The potential of utilising rs-fMRI data as biomarker in neurodegenerative disorders is also discussed in the literature (Hohenfeld, Werner, & Reetz, 2018). rs-fMRI is an fMRI technique that measures the low-frequency fluctuations in the BOLD signal while the subject is in the resting condition (not actively performing any task). Since the discovery of rs-fMRI (Biswal, Yetkin, Haughton, & Hyde, 1995), several methods have been developed to analyse rs-fMRI data (Lee, Smyser, & Shimony, 2013) and the possibility of deriving various rs-fMRI metrics has also been reported (Shehzad et al., 2009; Zhang, Han, Hu, Guo, & Liu, 2013; Zuo et al., 2010, 2013). In this exploratory analysis, the following rs-fMRI metrics were considered for comparison with other neuroelectric and neurometabolic measures:

- Regional homogeneity (ReHo) (Zang, Jiang, Lu, He, & Tian, 2004) is a voxel-based measure used to characterise the functional homogeneity of the rs-fMRI signal within a short range. ReHo weighs the degree of synchronisation between a given voxel and its nearest neighbouring voxels time series. Kendall's coefficient of concordance (KCC) (Stuart, 1956) is used as an index to measure the degree of synchronisation in ReHo analysis. Since the ReHo metric considers only neighbouring voxels, it depicts the strength of functional connectivity within neighbouring voxels. A voxel with a high ReHo value is functionally well connected with neighbouring voxels. ReHo analysis has been applied considerably in rs-fMRI data analysis (Long et al., 2008; Zang et al., 2004) and changes in ReHo values have also been reported in schizophrenia (Del Guerra et al., 2017; Liu et al., 2006), Alzheimer's disease (He et al., 2007) and in several other disorders.
- Degree centrality (DC) (Buckner et al., 2009; Joyce, Laurienti, Burdette, & Hayasaka, 2010) or global functional connectivity density (Tomasi & Volkow, 2012) is a functional connectivity measure, which estimates the number of direct functional connections between a given voxel and all the other voxels in the brain. Pearson's correlation coefficient is used as the measure to estimate DC. The DC metric considers all the voxels, and thus the value shown by the DC metric is the sum of local and long-range functional connectivity. Since the long-range voxels are comparatively high in number, the DC metric can be considered as a long-range functional connectivity measure. A voxel with a higher DC value means that this particular voxel is functionally well connected to many other voxels. DC has been largely studied to reveal the cortical functional hubs in the brain (Buckner et al., 2009; Zuo et al., 2012).
- Amplitude of low-frequency fluctuations (ALFFs) (Zang et al., 2007) and fractional amplitude of low-frequency fluctuations (fALFF) (Zou et al., 2008) are interrelated measures that quantify the amplitude of low-frequency oscillations (LFO), a fundamental feature of the rs-fMRI measurements. The ALFF measure of a

rs-fMRI voxel time series is defined as the total power within the low-frequency range between 0.01 and 0.1 Hz. Similarly, the fALFF measure of a rs-fMRI voxel time series is defined as the power within the low-frequency range (0.01–0.1 Hz) divided by the total power in the entire detectable frequency range. The ALFF and fALFF metrics only consider the time series of single voxels. Hence, these measures do not reveal functional relationships with other voxels. However, the ALFF metric describes the strength of LFO, while the fALFF metric describes the relative contribution of LFO to the whole frequency range. Thus, ALFF and fALFF characterise the slow fluctuations in the resting brain. A deviation in ALFF has been reported in children with attention deficit hyperactivity disorder (Zang et al., 2007) and is also associated with mild cognitive impairment (MCI) (Xi et al., 2012). Furthermore, variations in fALFF have been reported in relation to healthy ageing (Hu, Chao, Zhang, Ide, & Li, 2014). Since ALFF and fALFF are interrelated measures, only the fALFF measure is further considered in this study.

The ongoing glucose energy metabolism during the resting condition can be quantified using 2-[18F]fluoro-2-desoxy-D-glucose PET (FDG-PET) (e.g., Riedl et al., 2014). The glucose metabolism, measured via FDG-PET, mainly reflects local neuronal and synaptic activity (Berti, Mosconi, & Pupi, 2014; Sokoloff, 1981). The standardised uptake value (SUV) is a widely used semiquantitative measure of the FDG uptake in the tissue or organ of interest (Thie, 2004). FDG-PET SUV can be compared with rs-fMRI and neuroelectric measures. Using FDG-PET, it has been found that glucose metabolism is reduced in patients with Alzheimer's disease and MCI (Kennedy et al., 1995; Landau et al., 2011; Mosconi et al., 2005).

Neuroelectric signals arising from the functioning of large-scale neuronal networks in the brain can be accessed via multichannel EEG. The spatial distribution of active neurons or neuronal networks can be revealed by EEG scalp topography. Such topographies are found to be quasi-stable for periods of about 80–120 ms (Koenig et al., 2002; Lehmann & Skrandies, 1980) and these quasi-stable periods are known as EEG microstates (Katayama et al., 2007; Lehmann, 1990; Lehmann, Pascual-Marqui, & Michel, 2009). Thus, EEG microstates embody the summation of instantaneously active neuronal sources in the brain. Most of the rs-EEG studies have consistently identified four topographies (usually labelled as A, B, C and D) across the entire recording, with each of these topographies constituting a 'microstate map' (Khanna, Pascual-Leone, Michel, & Farzan, 2015; Koenig et al., 2002). The topographies observed in the microstate maps are right-frontal left-posterior (A), left-frontal right-posterior (B), midline frontal-occipital (C) and midline frontal (D). The functional interpretation of such observed microstate maps is based on the assumption that each map (topography) is generated by the coordinated activity of diverse neuronal assemblies. Transition of microstate maps may be regarded as sequential activation of various neuronal assemblies (Khanna et al., 2015). Changes in the frequency of occurrence, duration and transition patterns of microstates have been reported in various neuropsychiatric disorders, such as Alzheimer's disease (Dierks et al., 1997), schizophrenia (Andreou et al., 2014; Tomescu et al., 2014), Tourette's syndrome (Stevens, Günther, Lutzenberger, Bartels, & Müller, 1996) and similar mental disorders. Since the EEG microstates incorporate the signals from all electrodes to show the functional state of the whole brain via topographical maps, it was chosen for comparison with rs-fMRI and FDG-PET SUV.

A small number of studies have reported the relationship between EEG microstates and rs-fMRI (Britz, Van De Ville, & Michel, 2010; Musso, Brinkmeyer, Mobascher, Warbrick, & Winterer, 2010; Van De Ville, Britz, Michel, & Nikos Logothetis, 2010) on simultaneously recorded rs-EEG and fMRI. The work by Britz et al. (2010) concluded that the four typical microstates may represent the resting-state networks (RSNs). The work by Van De Ville et al. (2010) suggested the microstates as 'atoms of thoughts' (the shortest constituting elements of cognition). Similarly, Musso et al. (2010) showed that the microstates are able to elicit BOLD activation patterns in RSNs. However, these studies only reported results from bimodalities (EEG and fMRI) and did not consider the rs-fMRI metrics as explained above.

Given the advantages afforded by the facility of simultaneous trimodal measurements, this exploratory study aims to analyse the relationship between rs-fMRI metrics (ReHo, DC and fALFF), neurometabolic measures (FDG-PET SUV) and neuroelectric measures (EEG microstates). The analysis of relationship between the measures will be performed on the default mode network (DMN) region of the brain. The DMN region is one of the most prominent and one of the most robust neuronal networks. The DMN region includes regions such as the posterior cingulate, precuneus, inferior parietal cortex, orbitofrontal cortex, medial prefrontal cortex, ventral anterior cingulate, left dorsolateral prefrontal cortex, left parahippocampus, inferior temporal cortex, nucleus accumbens and the midbrain (Buckner, Andrews-Hanna, & Schacter, 2008; Raichle & Snyder, 2007). The DMN is believed to contribute to the baseline state of the brain and it appears to play a significant role in large-scale functional organisation of the brain (Raichle, 2015). Abnormalities in the DMN have been reported in various neurological and psychiatric disorders (Mingoia et al., 2012; Yao et al., 2014; Zhou et al., 2016). Moreover, the DMN has been shown as a potential biomarker for monitoring the therapeutic effects of meditation (Simon & Engström, 2015), chemotherapy-related brain injury (Kesler, 2014), Alzheimer's disease (Badhwar et al., 2017) and so forth. Considering these potential applications and widespread regions across the brain, the DMN is chosen for comparing microstates with rs-fMRI and neurometabolic measures.

To the best of the authors' knowledge, such comparison of EEG microstates with rs-MRI metrics and neurometabolic measures in the DMN region has not yet been reported on a simultaneously recorded trimodal data set. It is hoped that analysis of these multimodal measures, which represent diverse physiological information, will pave the way for understanding the complex behaviour of the brain in the resting condition and will help in developing new image-based biomarkers for the early detection and treatment monitoring of various neuropsychiatric disorders.

2 | METHODS

2.1 | Subjects

The trimodal data (MRI, FDG-PET and EEG) were recorded in a single scanning session using a 3T hybrid MR-BrainPET scanner system

(Siemens, Erlangen, Germany) (Herzog et al., 2011). The trimodal data were recorded from 11 healthy male volunteers of age 28.6 ± 3.4 years. The raw data set used in this study was taken from a previously published work (Shah et al., 2017). The study was approved by the Ethics Committee of the Medical Faculty of the RWTH Aachen University and the Federal Office for Radiation Protection (Bundesamt für Strahlenschutz). All methods used in this study were performed according to relevant guidelines and regulations. This study was conducted according to the Declaration of Helsinki and prior, written consent was obtained from all volunteers.

2.2 | Data acquisition

The data acquisition protocol for each modality is described below.

2.2.1 | MR data acquisition

The following MR sequences were included in the MR data acquisition protocol:

- Magnetisation-prepared rapid acquisition gradient-echo sequence (T1 weighted anatomical imaging sequence, repetition time (TR) = 2,250 ms, echo time (TE) = 3.03 ms, field-of-view (FOV) 256 × 256 × 176 mm^3, voxel size = 1 × 1 × 1 mm^3, flip angle (FA) = 9°, 176 sagittal slices and a GRAPPA acceleration factor of 2 with 70 autocalibration signal lines; and
- T2*-weighted echo planar imaging (TR = 2,200 ms, TE = 30 ms, FOV = 200 × 200 × 108 mm^3, voxel size = 3.125 × 3.125 × 3.0 mm^3, FA = 80°, number of slices = 36, number of volumes = 165).

2.2.2 | PET data acquisition

Subjects were instructed to fast overnight and to skip breakfast on the day of trimodal measurement. An intravenous line (IV-line) was inserted in the right arm before the measurement in order to inject the FDG. Fasting blood glucose level was determined prior to the measurement. FDG was injected (200 ± 30 MBq) as a single bolus injection via the IV-line while the volunteer was lying in the hybrid MR-BrainPET scanner. The acquisition of PET started simultaneously with the injection of the FDG tracer and occurred in list mode. PET data were iteratively reconstructed (3D OP-OSEM, 32 iterations and two subsets). The reconstructed images comprised 256 × 256 pixels and 153 slices (voxel size 1.25 mm^3, isotropic). The PET data reconstruction incorporated corrections for attenuation (Rota Kops, Hautzel, Herzog, Antoch, & Shah, 2015), random and scattered coincidences, dead time, radioactive decay and pile up. Since it is not possible to acquire attenuation information of the EEG cap, the attenuation map used for attenuation correction did not include the EEG cap; however, it was proven that the components used in the EEG cap causes inconsequential attenuation effects (Rajkumar et al., 2017).

2.2.3 | EEG data acquisition

Prior to the trimodal measurement, subjects were prepared for the EEG recording by having the EEG cap placed on the head, along with the application of electrolyte gel (Abralyt 2000; EasyCap GmbH, Herrsching, Germany) to reduce the impedance. The impedance of all recording electrodes was kept below 10 kΩ. The EEG data were recorded with a Brain Vision Recorder (Brain Products, Gilching, Germany) using a 32-channel MR compatible EEG. The EEG cap (BrainCap MR; EasyCap GmbH), consisting of 31 scalp electrodes, was positioned according to the 10–20 system, and had one additional electrode for recording the electrocardiogram (ECG). The sampling rate of the EEG recording was 5 kHz. The bandwidth of the recording was between 0.016 and 250 Hz. The rs (eyes closed) EEG data were recorded simultaneously during fMRI and PET data acquisition. The EEG data acquisition started exactly 50 min after PET tracer injection for each subject. Subjects were instructed to close their eyes and not to fall asleep during the rs measurement. The trimodal acquisition of the rs data lasted for about 6 min. The helium pump of the MRI system was switched off to avoid additional vibrations on both the EEG and MR system, and on the subject.

2.3 | Data analysis

One subject's data set was eliminated from further analysis due to the bad quality of the trimodal data (due to head motion in the scanner). Thus, only 10 subjects were included in the subsequent analysis.

2.3.1 | MR data

The rs-fMRI metrics (ReHo, DC, fALFF) were calculated using MATLAB-based software packages, SPM12 (http://www.fil.ion.ucl.ac.uk/spm/) and DPABI (Yan, Wang, Zuo, & Zang, 2016). The preprocessing steps performed on fMRI volumes before calculating the rs-fMRI metrics included the removal of the first 10 volumes of the total acquisition, slice time correction with respect to the middle slice (18th slice) of the functional image, realignment and nuisance covariates regression (NCR). The covariates for NCR included the head motion parameters calculated using Friston's 24 parameter model (Friston, Williams, Howard, Frackowiak, & Turner, 1996), mean signals from the whole brain white matter and cerebral spinal fluid as well as constant, linear and quadratic trends in the BOLD signals. Following these preprocessing steps, the functional connectivity measures for each subject were calculated in the subject's native image space. The processing steps performed to calculate each connectivity measure are described below. The fALFF measure was calculated within the low-frequency range of the BOLD fMRI signal between 0.01 and 0.1 Hz. Temporal filtering of BOLD fMRI signal between 0.01 and 0.08 Hz was performed only before DC and ReHo calculation. The ReHo connectivity measure was calculated over a cluster of 27 neighbouring voxels (Li, Kadivar, Pluta, Dunlop, & Wang, 2012) using KCC as the homogeneity metric. DC measure was computed with the Pearson correlation cut-off of 0.25 (p = .001). In order to perform inter-modality comparisons of rs-fMRI metrics, the calculated measures were linearly standardised into Z-values (Aiello et al., 2015) for each subject. Z-value standardisation was calculated by subtracting the mean whole brain voxel value from each voxel and then dividing the difference by the *SD* of the whole brain. The Z-value standardised connectivity measures were co-registered to the montreal neurological institute (MNI) standard space MNI152 (2 × 2 × 2 mm^3)) in order to perform inter-modality comparisons. Finally, the calculated rs-fMRI metrics were smoothed with a Gaussian kernel size of 3 mm along all three directions.

A mask of the DMN regions was generated by adding dorsal and ventral DMN regions, which were obtained from an atlas of 90 functional regions of interest (Shirer, Ryali, Rykhlevskaia, Menon, & Greicius, 2012). The generated mask of the DMN region is shown in Figure S1, Supporting Information. In order to further restrict the calculations to the grey matter (GM) regions, only the voxels within the GM region of the mask (which shows more than 50% probability of being GM) were considered (GM correction). A tissue segmented MNI152 ($2 \times 2 \times 2$ mm^3) template was used for GM correction. Finally, the voxel values within the DMN mask were extracted from the previously calculated fMRI metrics and a one-sample Kolmogorov–Smirnov test (KS test) was performed in order to verify normality. After confirming the normality of the extracted voxels, the mean values of ReHo, DC and fALFF were calculated. The calculated mean values were applied as rs-fMRI metrics for further comparison with neurometabolic and neuroelectric measures.

2.3.2 | PET data

The reconstructed PET images were smoothed with a Gaussian kernel of 3 mm size along all three directions and corrected for motion by considering the first frame of the whole acquisition as the reference using the PMOD (Version 3.5) software package. During the first 30 min, the uptake of FDG is reaching an equilibrium state; therefore, for further analysis, only the acquired PET data between 30 and 60 min post injection (six frames, 5 min each) were considered. The six PET images were averaged and an SUV map was calculated accounting for the injected dose and body weight of the considered subject. The FDG-PET SUV images were co-registered to the FDG-PET MNI ($2 \times 2 \times 2$ mm^3) template. The FDG-PET template in MNI space was obtained from a study by Della Rosa et al. (2014). Similar to the standardisation performed for rs-fMRI metrics, the MNI co-registered FDG-PET SUV images were also linearly standardised into Z-values. The voxel values within the FDG-PET SUV's DMN region were extracted using the DMN mask generated previously. A one-sample KS test was performed for the extracted values and the mean values of FDG-PET SUV within DNM regions were calculated. The mean FDG-PET SUV values within DMN region were used for further comparison with rs-fMRI metrics and neuroelectric measures.

2.3.3 | EEG data

The EEG data were processed using the MATLAB-based open source software package EEGLAB version 13 (Delorme & Makeig, 2004) and BrainVision Analyser (Version 2.02, Brain Products GmbH). The EEG data were analysed in two steps. In the first step, the data preprocessing was performed, in which the artefacts were removed, and in the second step, the microstates for each subject were calculated. The processing stages involved in each step are explained hereafter.

2.3.4 | EEG data preprocessing

The recorded EEG data were imported to EEGLAB and downsampled to 1,000 Hz. EEG data acquired simultaneously with fMRI are always heavily contaminated with gradient artefacts (GAs) and ballistocardiogram (BCG) artefacts. The GAs are added to the EEG signal due to switching of the gradient magnets in the MR system during fMRI acquisitions. BCG artefacts are always present during the entire acquisition of EEG data, due to the pulsatile flow of blood caused by the pumping action of heart.

The GAs were removed using FASTR tool (Niazy, Beckmann, Iannetti, Brady, & Smith, 2005) implemented in EEGLAB. After the GAs correction, the EEG data were band-pass filtered using a Hamming windowed sinc finite impulse response filter with a lower cut-off frequency of 2 Hz and a higher cut-off frequency of 8 Hz for the ECG channel and 20 Hz for the remaining EEG channels (the filter order was calculated automatically by the *eegfiltnew* function implemented in EEGLAB). The recorded R peaks in the ECG channel data, along with the EEG data, were semimanually detected using BrainVision Analyser software. The EEG data were again imported to EEGLAB and the BCG artefacts were removed using the FMRIB tool (Kim, Yoon, & Park, 2004) implemented in EEGLAB. The artefacts in EEG data, due to eye movement, were corrected using a blind source separation method (Go'mez-Herrerol et al., 2006). Bad channels in the EEG data, resulting from the loose contact between the EEG electrode and the scalp, were removed. An independent component analysis (ICA)-based decomposition was performed using the extended Infomax algorithm (Lee, Girolami, & Sejnowski, 1999) on all the EEG channels. The ICA decomposition yielded 31 independent components. The noisy components were detected and removed using the Multiple Artifact Rejection Algorithm (Winkler, Haufe, & Tangermann, 2011). The artefact removed EEG data were epoched with respect to the TR of the fMRI acquisition, which was 2.2 s. The first 10 epochs were removed from the EEG data, as performed for the fMRI volumes. The epoched EEG data were examined for movement or other residual artefacts and noisy epochs were removed.

2.3.5 | Microstate analysis

The microstates in artefact-free EEG data were analysed using the Microstate plugin (http://www.thomaskoenig.ch/index.php/software/microstates-in-eeglab) implementation in EEGLAB. The global field power (GFP) of the multichannel EEG data represents the global brain activity (Lehmann & Skrandies, 1980). The EEG topographies were found to be stable around the maxima of the GFP (GFP peaks) (Koenig et al., 2002). Thus, the GFP peaks were calculated for each subject first. All EEG topographical maps marked as GFP peaks were extracted and spatial clustering was performed using a modified atomised and agglomerate hierarchical clustering (AAHC) algorithm (Tibshirani & Walther, 2005). The AAHC algorithm was set to identify dominant EEG topographical maps for each subject. In the next step, the EEG topographical maps, identified in every single subject, were submitted to the same modified AAHC algorithm to identify the dominant EEG topographical maps (group template) across all subjects. The group template topographical maps were then manually sorted in to microstates A, B, C and D, as reported in previous rs-microstate studies (Khanna et al., 2015; Koenig et al., 2002). Finally, the EEG topographical maps, identified for each subject, were also sorted into microstates A, B, C and D, as in group template maps. The sorting of microstate maps at subject level was performed via the calculation of the spatial correlation between the sorted group template maps and the EEG topographical maps identified for each subject. The mean

GFP in each of the four microstate maps for each subject was calculated and used in the subsequent analysis.

2.3.6 | Statistics

In order to perform statistical comparison between the results obtained from each modality, the Spearman correlation coefficient was calculated between the mean GFP of the four microstate maps and the mean rs-fMRI metrics extracted from the DMN masks for each subject. The family-wise error rate, due to multiple comparisons, was controlled via a permutation test (Groppe, Urbach, & Kutas, 2011). Exactly 10^5 permutations were carried out for each comparison (correlation of each microstate to the mean rs-fMRI metrics) and the *p*-value was adjusted using the 'max statistics' method reported by Groppe et al. (2011). Similarly, a Spearman correlation coefficient with 10^5 permutations was calculated between the mean GFP of the four microstate maps and the mean FDG-PET SUV extracted from the DMN masks for each subject.

3 | RESULTS

Simultaneous trimodal data acquisition was successfully performed. The fMRI metrics and FDG-PET SUV were calculated as described above and the voxel values within the DMN mask were extracted. The one-sample KS test revealed that the extracted voxel values for each of the fMRI metrics and FDG-PET SUV were normally distributed. Thus, the mean of the fMRI metrics and FDG-PET SUV within the DMN region was calculated for each subject. The calculated rs-fMRI metrics and FDG-PET SUV maps averaged across all the 10 subjects are shown in Figure 1.

Artefacts due to magnetic field gradient, BCG, eye movement, head movement and other sources in the raw EEG data were successfully removed and verified via visual inspection. The four prominent microstates, widely reported in other rs-EEG studies, were identified for each subject. The sorted group template microstate across all subjects is shown in Figure 2.

The mean GFP of each microstate was calculated and submitted for further statistical comparison with rs-fMRI metrics and neurometabolic measure. The Spearman correlation coefficients and the adjusted *p*-value via 10^5 permutations for each comparison are plotted in Figure S2, Supporting Information. FDG-PET SUV as well as rs-fMRI metrics, such as ReHO, and fALFF, did not show significant correlations with the microstates. The DC metric showed a significant positive correlation with microstate C (Spearman correlation coefficient $r_s = 0.73$, adjusted $p = .01$), as shown in Figure 3.

4 | DISCUSSION AND CONCLUSIONS

In this exploratory analysis, simultaneously acquired trimodal data were processed and analysed in order to investigate the relationship between rs-fMRI metrics, neurometabolic and neuroelectric measures. Each modality characterises complimentary physiological information. The rs-fMRI metrics and FDG-PET SUV measure reveal distinct information about the functioning of the human brain. Furthermore, given that various groups have already explored and reported the relationship between rs-fMRI metrics and FDG-PET SUV measure

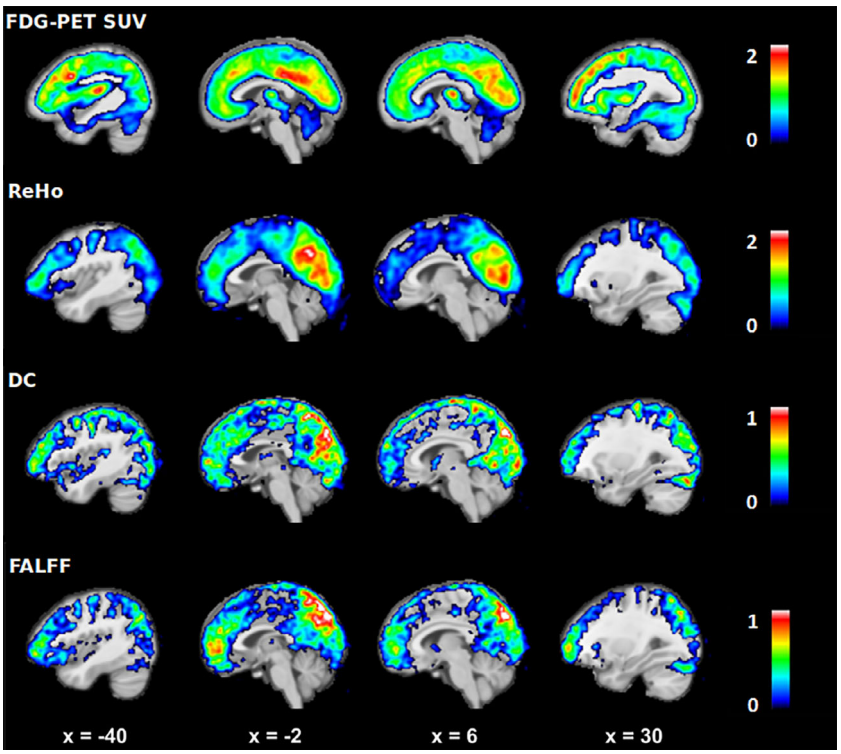

FIGURE 1 FDG-PET standardised uptake value (SUV; upper row) and resting state fMRI metrics such as regional homogeneity (ReHo), degree of centrality (DC) and fractional amplitude of low-frequency fluctuations (fALFFs). Sagittal slices ($x = -40, -2, 6$ and 30 in MNI space), averaged across all the 10 subjects, are shown

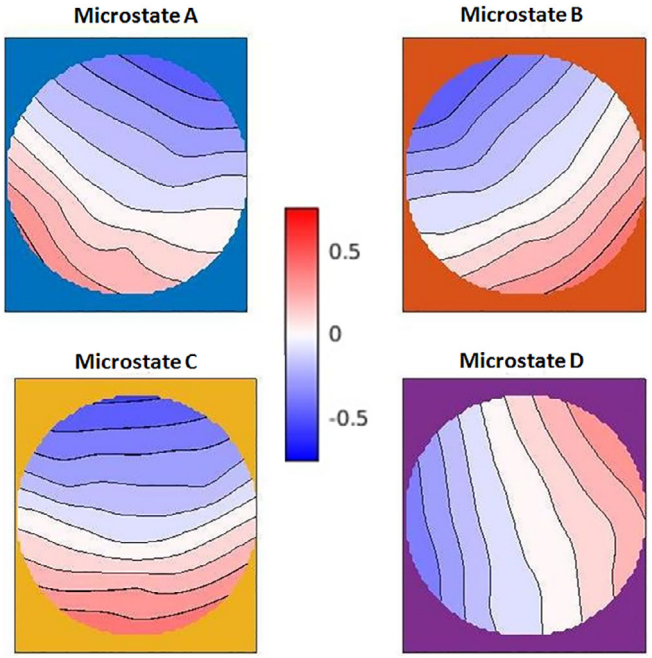

FIGURE 2 The four prominent microstates (group template) identified and sorted across the 10 subjects

(Aiello et al., 2015; Riedl et al., 2014), this study mainly focused on utilising the advantage of simultaneously recorded EEG data for comparison with rs-fMRI metrics and FDG-PET SUV measure. Each of the microstates calculated from EEG data also represents the global functional state of the brain via topographical plots. The four microstates, widely identified in various rs-studies (Koenig et al., 2002; Dietrich Lehmann et al., 2005; Stevens, Lutzenberger, Bartels, Strik, & Lindner, 1997; Yuan, Zotev, Phillips, Drevets, & Bodurka, 2012), reflect different underlying functional networks.

The rs-fMRI metrics, such as ReHo, and fALFF in the DMN region, did not show significant correlation with either of the microstates. This may be due to the fact that ReHo, and fALFF depict either local connectivity or voxel level fluctuations of LFO, whereas the microstates represent the global functional state of the brain.

In contrast, the long-range rs-fMRI functional connectivity metric DC showed a significant positive correlation with microstate C (Figure 3). Various studies have shown that a major portion of the DMN is reflected in microstate C (Britz et al., 2010; Custo et al., 2017; Michel & Koenig, 2018; Seitzman et al., 2017). Our finding of a significant correlation between the DC metric in the DMN region and microstate C in the absence of correlations with short-range measures highlight the importance of long-range connections. These long-range connections are most vulnerable to disease conditions (Mingoia et al., 2012; Yao et al., 2014; Zhou et al., 2016). Studies have reported on the extensive structural and functional connections between the DMN regions in the frontal and occipital lobes (Khalsa, Mayhew, Chechlacz, Bagary, & Bagshaw, 2014).

The neurometabolic measure, FDG-PET SUV in the DMN region, did not show significant correlations with the microstates. A small number of groups have already reported the inverse correlation between FDG-PET and EEG frequency bands. For instance, a study by Oakes et al. (2004) have demonstrated the existence of negative correlations between localised EEG power in the θ (6.5–8 Hz), α1 (8.5–10 Hz) and β1 (12.5–18 Hz) frequency bands and metabolic activity as measured via FDG-PET. In another study, negative correlations between the δ band (0.5–4 Hz) of electrocorticography (an invasive procedure to record electrophysiology directly from the cerebral cortex) and FDG-PET in patients with epilepsy (Nishida et al., 2008) were shown. Similarly, negative correlations between the δ (1.5–4 Hz) frequency band of EEG and regional cerebral blood flow were also reported in healthy volunteers (Hofle et al., 1997). In addition to these studies, other works have also focussed on combined EEG and FDG-PET analysis in neurological and psychiatric disorders. A relationship between rs-EEG rhythms and hypometabolism in subjects with Alzheimer's disease has been recently reported (Babiloni et al., 2016). Another study also reported associations between EEG high and low alpha power ratio and cortical glucose metabolism accessed via FDG-PET in subjects with MCI (Moretti et al., 2017). All of these studies show an inverse relationship between EEG and glucose metabolism, as accessed via FDG-PET, both in healthy subjects and subjects with disorders. All the findings reported above are interesting and interpretable, but cannot be used for direct comparison with the results obtained in this exploratory analysis, since this is the first exploratory study to investigate the relationship between neuroelectric signals via microstates and neurometabolic signals via FDG-PET. GFPs obtained from most of the microstates showed negative correlations with SUV of FDG-PET, as shown in Figure S2, Supporting Information.

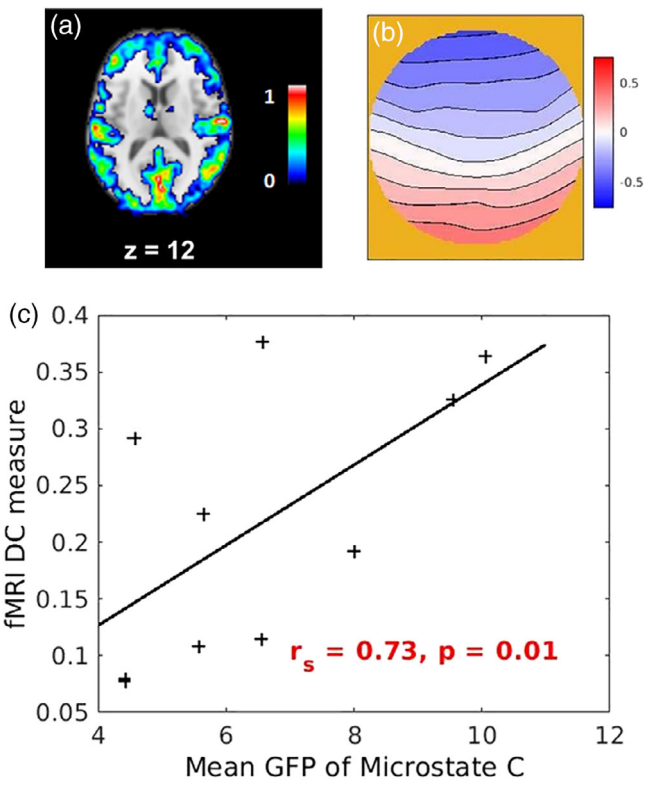

FIGURE 3 Correlation plot between mean GFP of microstate C and rs-fMRI DC metric (c). For the purpose of visual observation the axial slice (*z* = 12 in MNI space) of rs-fMRI DC metric (a) and EEG microstate C (b) are shown in the top row

However, the correlations are not significant, which may be due to the limited number of subjects included in this exploratory analysis. Please note that the exposure to radioactivity to healthy volunteers is only allowed in a very narrow legal framework and requires the sample size calculation only at the lowest possible range. The results from the comparison of microstates and FDG-PET SUV tend to be in agreement with the classical perspective that EEG fluctuations may be inversely related to the activation of the brain (Davidson et al., 2000).

The DMN regions are found to be disrupted anatomically as well as functionally and are reported to play a critical role in the pathophysiology of various psychiatric and neurological disorders (Broyd et al., 2009; Hu et al., 2017; Mohan et al., 2016). In this foremost exploratory analysis to underpin the relationship between neuroelectric measures of the rs-brain, as determined via microstates, with rs-fMRI metrics and FDG-PET SUV measure highlights the importance of long-range connections. The DC metric from rs-fMRI, which was found to be significantly positively correlated with microstate C, was reported to be altered in various mental disorders, such as major depressive disorder (Murrough et al., 2016), schizophrenia and bipolar spectrum disorders (Skåtun et al., 2016). Similarly, variations in microstate C have been reported in various mental disorders such as schizophrenia (Lehmann et al., 2005; Tomescu et al., 2014), frontotemporal dementia (Nishida et al., 2013) and panic disorder (Kikuchi et al., 2007). It is interesting to note from the aforementioned reported results that both the DC metric from rs-fMRI and microstate C show alterations in a broad spectrum of disorders. Combined analysis of similar or the same measurement from simultaneously acquired data in patients with such disorders can potentially pave the way for understanding pathophysiology and developing the rs-fMRI image-based or electrophysiology-based biomarkers for the diagnosis, treatment and monitoring of neurological disorders. Another important finding in this study is the fact that the FDG-PET SUV measure, which was obtained from simultaneously recorded trimodal data, also shows a trend of inverse relationship with the neuroelectric measure, microstate. Previous studies using FDG-PET have shown alterations in cerebral glucose metabolism in disorders such as schizophrenia (Kim et al., 2017; Seethalakshmi et al., 2006), dementia (Mosconi et al., 2009; Shivamurthy, Tahari, Marcus, & Subramaniam, 2015) and in other psychiatric disorders (Newberg, Alavi, & Reivich, 2002; Newberg, Monti, Moss, & Alavi, 2012). Even though the FDG-PET measure is performed via a minimally invasive procedure, obtaining such a neurometabolic measure along with other modalities will improve diagnostic accuracy and may also help in early diagnosis (Polikar et al., 2010). The significant results and the trends prompt further research for replication and the transfer to different patient populations to exploit the mutual clinical potential.

ACKNOWLEDGMENTS

This study is part of the doctoral thesis (Dr. rer. medic.) of Ravichandran Rajkumar at the Medical Faculty of the RWTH Aachen University, Germany. The authors gratefully thank Dr. Jorge Arrubla for assistance in trimodal human data acquisition. The authors would like to thank Prof. Thomas Koenig (University Hospital of Psychiatry, Bern, Switzerland) for providing support with EEG Lab Microstate plug-in. The authors would also like to thank Andrea Muren, Cornelia Frey, Silke Frensch and Suzanne Schaden for their technical assistance. Finally, the authors would like to acknowledge their gratitude to Claire Rick and Joshua Lewis Bierbrier for proofreading the manuscript. This study was in part supported by the EU FP7 funded project TRIMAGE (Nr. 602621).

ORCID

Ravichandran Rajkumar https://orcid.org/0000-0001-5875-5316
Ezequiel Farrher https://orcid.org/0000-0003-2902-8667
Jörg Mauler https://orcid.org/0000-0003-4937-0355
Praveen Sripad https://orcid.org/0000-0001-6361-2571
Elena Rota Kops https://orcid.org/0000-0002-0959-9457
Jürgen Dammers https://orcid.org/0000-0003-1526-6592
Christoph Lerche https://orcid.org/0000-0003-2749-2108
Karl-Josef Langen https://orcid.org/0000-0003-1101-5075
N. Jon Shah https://orcid.org/0000-0002-8151-6169
Irene Neuner https://orcid.org/0000-0002-5164-8873

REFERENCES

Abreu, R., Leal, A., & Figueiredo, P. (2018). EEG-informed fMRI: A review of data analysis methods. *Frontiers in Human Neuroscience*, *12*, 29. http://doi.org/10.3389/fnhum.2018.00029

Aiello, M., Salvatore, E., Cachia, A., Pappatà, S., Cavaliere, C., Prinster, A., … Quarantelli, M. (2015). NeuroImage relationship between simultaneously acquired resting-state regional cerebral glucose metabolism and functional MRI: A PET/MR hybrid scanner study. *NeuroImage*, *113*, 111–121. http://doi.org/10.1016/j.neuroimage.2015.03.017

Andreou, C., Faber, P. L., Leicht, G., Schoettle, D., Polomac, N., Hanganu-Opatz, I. L., … Mulert, C. (2014). Resting-state connectivity in the prodromal phase of schizophrenia: Insights from EEG microstates. *Schizophrenia Research*, *152*(2–3), 513–520. http://doi.org/10.1016/j.schres.2013.12.008

Babiloni, C., Del Percio, C., Caroli, A., Salvatore, E., Nicolai, E., Marzano, N., … Soricelli, A. (2016). Cortical sources of resting state EEG rhythms are related to brain hypometabolism in subjects with Alzheimer's disease: An EEG-PET study. *Neurobiology of Aging*, *48*, 122–134. http://doi.org/10.1016/j.neurobiolaging.2016.08.021

Badhwar, A. P., Tam, A., Dansereau, C., Orban, P., Hoffstaedter, F., & Bellec, P. (2017). Resting-state network dysfunction in Alzheimer's disease: A systematic review and meta-analysis. *Alzheimer's & Dementia*, *8*, 73–85. http://doi.org/10.1016/j.dadm.2017.03.007

Bai, Y., Xia, X., & Li, X. (2017). A review of resting-state electroencephalography analysis in disorders of consciousness. *Frontiers in Neurology*, *8*, 471. http://doi.org/10.3389/fneur.2017.00471

Bayouth, J. E., Casavant, T. L., Graham, M. M., Sonka, M., Muruganandham, M., & Buatti, J. M. (2011). Image-based biomarkers in clinical practice. *Seminars in Radiation Oncology*, *21*, 157–166. http://doi.org/10.1016/j.semradonc.2010.11.003

Berti, V., Mosconi, L., & Pupi, A. (2014). Brain: Normal variations and benign findings in fluorodeoxyglucose-PET/computed tomography imaging. *PET Clinics*, *9*(2), 129–140. http://doi.org/10.1016/j.cpet.2013.10.006

Biswal, B., Yetkin, F. Z., Haughton, V. M., & Hyde, J. S. (1995). Functional connectivity in the motor cortex of resting human brain using echo-planar MRI. *Magnetic Resonance in Medicine*, *34*(4), 537–541.

Boellaard, R. (2008). Standards for PET image acquisition and quantitative data analysis. *Journal of Nuclear Medicine*, *50*(Suppl. 1), 11S–20S. http://doi.org/10.2967/jnumed.108.057182

Bowman, F. D., Guo, Y., & Derado, G. (2007). Statistical approaches to functional neuroimaging data. *Neuroimaging Clinics of North America*, *17*, 441–458. http://doi.org/10.1016/j.nic.2007.09.002

Britz, J., Van De Ville, D., & Michel, C. M. (2010). BOLD correlates of EEG topography reveal rapid resting-state network dynamics. *NeuroImage*, *52*, 1162–1170. http://doi.org/10.1016/j.neuroimage.2010.02.052

Broyd, S. J., Demanuele, C., Debener, S., Helps, S. K., James, C. J., & Sonuga-Barke, E. J. S. (2009). Default-mode brain dysfunction in mental disorders: A systematic review. *Neuroscience and Biobehavioral Reviews*, *33*(3), 279–296. http://doi.org/10.1016/j.neubiorev.2008.09.002

Buckner, R. L., Andrews-Hanna, J. R., & Schacter, D. L. (2008). The brain's default network: Anatomy, function, and relevance to disease. *Annals of New York Academy of Sciences*, *1124*, 1–38. http://doi.org/10.1196/annals.1440.011

Buckner, R. L., Sepulcre, J., Talukdar, T., Krienen, F. M., Liu, H., Hedden, T., … Johnson, K. A. (2009). Cortical hubs revealed by intrinsic functional connectivity: Mapping, assessment of stability, and relation to Alzheimer's disease. *The Journal of Neuroscience*, *29*(6), 1860–1873. http://doi.org/10.1523/JNEUROSCI.5062-08.2009

Custo, A., Van De Ville, D., Wells, W. M., Tomescu, M. I., Brunet, D., & Michel, C. M. (2017). Electroencephalographic resting-state networks: Source localization of microstates. *Brain Connectivity*, *7*(10), 671–682. http://doi.org/10.1089/brain.2016.0476

Davidson, R.J., Jackson, D.C., Larson, C.L. Human electroencephalography. In: Cacioppo, J. T., Tassinary, L. G., Berntson, G. G., editors. *Handbook of psychophysiology*. *2*. Cambridge, UK: Cambridge University Press; 2000. pp. 27–52.

Del Guerra, A., Ahmad, S., Avram, M., Belcari, N., Berneking, A., Biagi, L., … Ziegler, S. (2017). TRIMAGE: A dedicated trimodality (PET/MR/EEG) imaging tool for schizophrenia. *Federation Proceedings*, *50*, 7–20. http://doi.org/10.1016/J.EURPSY.2017.11.007

Della Rosa, P. A., Cerami, C., Gallivanone, F., Prestia, A., Caroli, A., Castiglioni, I., … Perani, D. (2014). A Standardized [18F]-FDG-PET Template for Spatial Normalization in Statistical Parametric Mapping of Dementia. *Neuroinformatics*, *12*(4), 575–59. http://doi.org/10.1007/s12021-014-9235-4

Delorme, A., & Makeig, S. (2004). EEGLAB: An open source toolbox for analysis of single-trial EEG dynamics including independent component analysis. *Journal of Neuroscience Methods*, *134*, 9–21. http://doi.org/10.1016/j.jneumeth.2003.10.009

Dierks, T., Jelic, V., Julin, P., Maurer, K., Wahlund, L. O., Almkvist, O., … Winblad, B. (1997). EEG-microstates in mild memory impairment and Alzheimer's disease: Possible association with disturbed information processing. *Journal of Neural Transmission*, *104*(4–5), 483–495. http://doi.org/10.1007/BF01277666

Friston, K. J., Williams, S., Howard, R., Frackowiak, R. S. J., & Turner, R. (1996). Movement-related effects in fMRI time-series. *Magnetic Resonance in Medicine*, *35*(3), 346–355. http://doi.org/10.1002/mrm.1910350312

Goldman, R. I., Stern, J. M., Engel, J., & Cohen, M. S. (2000). Acquiring simultaneous EEG and functional MRI. *Clinical Neurophysiology*, *111*(11), 1974–1980. http://doi.org/10.1016/S1388-2457(00)00456-9

Golkowski, D., Merz, K., Mlynarcik, C., Kiel, T., Schorr, B., Lopez-Rolon, A., … Ilg, R. (2017). Simultaneous EEG–PET–fMRI measurements in disorders of consciousness: An exploratory study on diagnosis and prognosis. *Journal of Neurology*, *264*(9), 1986–1995. http://doi.org/10.1007/s00415-017-8591-z

Go'mez-Herrerol, G., Clercq, W. De, Anwara, H., Kara, O., Egiazarian, K., Huffel, S. Van, & Paesschen, W. Van. (2006). *Automatic removal of ocular artifacts in the EEG without an EOG Reference Channel*. J. R. Sveinsson (Ed.), Proceedings of the 7th Nordic Signal Processing Symposium (NORSIG 2006) (pp. 130-133), 7-9 June 2006, Reykjavik, Iceland. https://doi.org/10.1109/NORSIG.2006.275210

Groppe, D. M., Urbach, T. P., & Kutas, M. (2011). Mass univariate analysis of event-related brain potentials/fields I: A critical tutorial review. *Psychophysiology*, *48*, 1711–1725. http://doi.org/10.1111/j.1469-8986.2011.01273.x

Hampel, H., Teipel, S. J., Alexander, G. E., Pogarell, O., Rapoport, S. I., & Möller, H. J. (2002). In vivo imaging of region and cell type specific neocortical neurodegeneration in Alzheimer's disease: Perspectives of MRI derived corpus callosum measurement for mapping disease progression and effects of therapy. Evidence from studies with MRI, EEG and PET. *Journal of Neural Transmission*, *109*(5–6), 837–855. http://doi.org/10.1007/s007020200069

He, Y., Wang, L., Zang, Y., Tian, L., Zhang, X., Li, K., & Jiang, T. (2007). Regional coherence changes in the early stages of Alzheimer's disease: A combined structural and resting-state functional MRI study. *NeuroImage*, *35*(2), 488–500. http://doi.org/10.1016/j.neuroimage.2006.11.042

Herzog, H., Langen, K. J., Weirich, C., Rota Kops, E., Kaffanke, J., Tellmann, L., … Shah, N. J. (2011). High resolution BrainPET combined with simultaneous MRI. *Nuklearmedizin*, *50*(2), 74–82. http://doi.org/10.3413/Nukmed-0347-10-09

Hofle, N., Paus, T., Reutens, D., Fiset, P., Gotman, J., Evans, A. C., & Jones, B. E. (1997). Regional cerebral blood flow changes as a function of delta and spindle activity during slow wave sleep in humans. *Journal of Neuroscience*, *17*(12), 4800–4808.

Hohenfeld, C., Werner, C. J., & Reetz, K. (2018). Resting-state connectivity in neurodegenerative disorders: Is there potential for an imaging biomarker? *NeuroImage: Clinical*, *18*, 849–870. http://doi.org/10.1016/j.nicl.2018.03.013

Hu, M.-L., Zong, X.-F., Mann, J. J., Zheng, J.-J., Liao, Y.-H., Li, Z.-C., … Tang, J.-S. (2017). A review of the functional and anatomical default mode network in schizophrenia. *Neuroscience Bulletin*, *33*(1), 73–84. http://doi.org/10.1007/s12264-016-0090-1

Hu, S., Chao, H. H. A., Zhang, S., Ide, J. S., & Li, C. S. R. (2014). Changes in cerebral morphometry and amplitude of low-frequency fluctuations of BOLD signals during healthy aging: Correlation with inhibitory control. *Brain Structure and Function*, *219*(3), 983–994. http://doi.org/10.1007/s00429-013-0548-0

Hur, Y. J., Lee, J. D. J. S., Lee, J. D. J. S., Yun, M. J., & Kim, H. D. (2013). Quantitative analysis of simultaneous EEG features during PET studies for childhood partial epilepsy. *Yonsei Medical Journal*, *54*(3), 572–577. http://doi.org/10.3349/ymj.2013.54.3.572

Huster, R. J., Debener, S., Eichele, T., & Herrmann, C. S. (2012). Methods for simultaneous EEG-fMRI: An introductory review. *The Journal of Neuroscience*, *32*(18), 6053–6060. http://doi.org/10.1523/JNEUROSCI.0447-12.2012

Joyce, K. E., Laurienti, P. J., Burdette, J. H., & Hayasaka, S. (2010). A new measure of centrality for brain networks. *PLoS One*, *5*(8), e12200. http://doi.org/10.1371/journal.pone.0012200

Katayama, H., Gianotti, L. R. R., Isotani, T., Faber, P. L., Sasada, K., Kinoshita, T., & Lehmann, D. (2007). Classes of multichannel EEG microstates in light and deep hypnotic conditions. *Brain Topography*, *20*(1), 7–14. http://doi.org/10.1007/s10548-007-0024-3

Kennedy, A. M., Frackowiak, R. S. J., Newman, S. K., Bloomfield, P. M., Seaward, J., Roques, P., … Rossor, M. N. (1995). Deficits in cerebral glucose metabolism demonstrated by positron emission tomography in individuals at risk of familial Alzheimer's disease. *Neuroscience Letters*, *186*(1), 17–20. http://doi.org/10.1016/0304-3940(95)11270-7

Kesler, S. R. (2014). Default mode network as a potential biomarker of chemotherapy-related brain injury. *Neurobiology of Aging*, *35*, S11–S19. http://doi.org/10.1016/j.neurobiolaging.2014.03.036

Khalsa, S., Mayhew, S. D., Chechlacz, M., Bagary, M., & Bagshaw, A. P. (2014). The structural and functional connectivity of the posterior cingulate cortex: Comparison between deterministic and probabilistic tractography for the investigation of structure-function relationships. *NeuroImage*, *102*(P1), 118–127. http://doi.org/10.1016/j.neuroimage.2013.12.022

Khanna, A., Pascual-Leone, A., Michel, C. M., & Farzan, F. (2015). Microstates in resting-state EEG: Current status and future directions. *Neuroscience & Biobehavioral Review*, *49*, 105–113. http://doi.org/10.1016/j.neubiorev.2014.12.010

Kikuchi, M., Koenig, T., Wada, Y., Higashima, M., Koshino, Y., Strik, W., & Dierks, T. (2007). Native EEG and treatment effects in neuroleptic-naïve schizophrenic patients: Time and frequency domain approaches. *Schizophrenia Research*, *97*(1–3), 163–172. http://doi.org/10.1016/j.schres.2007.07.012

Kim, J. H., Kim, J. H., Son, Y. D., Joo, Y. H., Lee, S. Y., Kim, H. K., & Woo, M. K. (2017). Altered interregional correlations between serotonin transporter availability and cerebral glucose metabolism in schizophrenia: A high-resolution PET study using [11C]DASB and [18F]FDG.

Schizophrenia Research, *182*, 55–65. http://doi.org/10.1016/j.schres.2016.10.020

Kim, K. H., Yoon, H. W., & Park, H. W. (2004). Improved ballistocardiac artifact removal from the electroencephalogram recorded in fMRI. *Journal of Neuroscience Methods*, *135*(1–2), 193–203. http://doi.org/10.1016/j.jneumeth.2003.12.016

Koenig, T., Prichep, L., Lehmann, D., Sosa, P. V., Braeker, E., Kleinlogel, H., … John, E. R. (2002). Millisecond by millisecond, year by year: Normative EEG microstates and developmental stages. *NeuroImage*, *16*(1), 41–48. http://doi.org/10.1006/nimg.2002.1070

Landau, S. M., Harvey, D., Madison, C. M., Koeppe, R. A., Reiman, E. M., Foster, N. L., … Jagust, W. J. (2011). Associations between cognitive, functional, and FDG-PET measures of decline in AD and MCI. *Neurobiology of Aging*, *32*(7), 1207–1218. http://doi.org/10.1016/j.neurobiolaging.2009.07.002

Laruelle, M., Iyer, R. N., Al-Tikriti, M. S., Zea-Ponce, Y., Malison, R., Zoghbi, S. S., … Bradberry, C. W. (1997). Microdialysis and SPECT measurements of amphetamine-induced dopamine release in nonhuman primates. *Synapse*, *25*(1), 1–14. http://doi.org/10.1002/(SICI)1098-2396(199701)25:1<1::AID-SYN1>3.0.CO;2-H

Lee, M. H., Smyser, C. D., & Shimony, J. S. (2013). Resting-state fMRI: A review of methods and clinical applications. *AJNR. American Journal of Neuroradiology*, *34*(10), 1866–1872. http://doi.org/10.3174/ajnr.A3263

Lee, T. W., Girolami, M., & Sejnowski, T. J. (1999). Independent component analysis using an extended infomax algorithm for mixed subgaussian and supergaussian sources. *Neural Computation*, *11*(2), 417–441.

Lehmann, D. (1990). Past, present and future of topographic mapping. *Brain Topography*, *3*(1), 191–202. http://doi.org/10.1007/BF01128876

Lehmann, D., Faber, P. L., Galderisi, S., Herrmann, W. M., Kinoshita, T., Koukkou, M., … Koenig, T. (2005). EEG microstate duration and syntax in acute, medication-naïve, first-episode schizophrenia: A multi-center study. *Psychiatry Research: Neuroimaging*, *138*(2), 141–156. http://doi.org/10.1016/j.pscychresns.2004.05.007

Lehmann, D., Pascual-Marqui, R., & Michel, C. (2009). EEG microstates. *Scholarpedia*, *4*(3), 7632. http://doi.org/10.4249/scholarpedia.7632

Lehmann, D., & Skrandies, W. (1980). Reference-free identification of components of checkerboard-evoked multichannel potential fields. *Electroencephalography and Clinical Neurophysiology*, *48*(6), 609–621. http://doi.org/10.1016/0013-4694(80)90419-8

Li, Z., Kadivar, A., Pluta, J., Dunlop, J., & Wang, Z. (2012). Test-retest stability analysis of resting brain activity revealed by blood oxygen level-dependent functional MRI. *Journal of Magnetic Resonance Imaging*, *36*(2), 344–354. http://doi.org/10.1002/jmri.23670

Liu, H., Liu, Z., Liang, M., Hao, Y., Tan, L., Kuang, F., … Jiang, T. (2006). Decreased regional homogeneity in schizophrenia: A resting state functional magnetic resonance imaging study. *Neuroreport*, *17*(1), 19–22. http://doi.org/10.1097/01.wnr.0000195666.22714.35

Liu, S., Cai, W., Liu, S., Zhang, F., Fulham, M., Feng, D., … Kikinis, R. (2015). Multimodal neuroimaging computing: A review of the applications in neuropsychiatric disorders. *Brain Informatics*, *2*(3), 167–180. http://doi.org/10.1007/s40708-015-0019-x

Long, X.-Y., Zuo, X.-N., Kiviniemi, V., Yang, Y., Zou, Q.-H., Zhu, C.-Z., … Zang, Y.-F. (2008). Default mode network as revealed with multiple methods for resting-state functional MRI analysis. *Journal of Neuroscience Methods*, *171*(2), 349–355. http://doi.org/10.1016/j.jneumeth.2008.03.021

Michel, C. M., & Koenig, T. (2018). EEG microstates as a tool for studying the temporal dynamics of whole-brain neuronal networks: A review. *NeuroImage*, *180*, 577–593. http://doi.org/https://doi.org/10.1016/j.neuroimage.2017.11.062

Mingoia, G., Wagner, G., Langbein, K., Maitra, R., Smesny, S., Dietzek, M., … Nenadic, I. (2012). Default mode network activity in schizophrenia studied at resting state using probabilistic ICA. *Schizophrenia Research*, *138*, 143–149. http://doi.org/10.1016/j.schres.2012.01.036

Mohan, A., Roberto, A. J., Mohan, A., Lorenzo, A., Jones, K., Carney, M. J., … Lapidus, K. A. B. (2016). The significance of the default mode network (DMN) in neurological and neuropsychiatric disorders: A review. *The Yale Journal of Biology and Medicine*, *89*(1), 49–57.

Moretti, D. V., Pievani, M., Pini, L., Guerra, U. P., Paghera, B., & Frisoni, G. B. (2017). Cerebral pet glucose hypometabolism in subjects with mild cognitive impairment and higher EEG high alpha/low alpha frequency power ratio. *Neurobiology of Aging*, *58*, 213–224. http://doi.org/10.1016/j.neurobiolaging.2017.06.009

Mosconi, L., Mistur, R., Switalski, R., Tsui, W. H., Glodzik, L., Li, Y., … De Leon, M. J. (2009). FDG-PET changes in brain glucose metabolism from normal cognition to pathologically verified Alzheimer's disease. *European Journal of Nuclear Medicine and Molecular Imaging*, *36*(5), 811–822. http://doi.org/10.1007/s00259-008-1039-z

Mosconi, L., Tsui, W. H., De Santi, S., Li, J., Rusinek, H., Convit, A., … De Leon, M. J. (2005). Reduced hippocampal metabolism in MCI and AD: Automated FDG-PET image analysis. *Neurology*, *64*(11), 1860–1867. http://doi.org/10.1212/01.WNL.0000163856.13524.08

Murrough, J. W., Abdallah, C. G., Anticevic, A., Collins, K. A., Geha, P., Averill, L. A., … Charney, D. S. (2016). Reduced global functional connectivity of the medial prefrontal cortex in major depressive disorder. *Human Brain Mapping*, *37*(9), 3214–3223. http://doi.org/10.1002/hbm.23235

Musso, F., Brinkmeyer, J., Mobascher, A., Warbrick, T., & Winterer, G. (2010). Spontaneous brain activity and EEG microstates. A novel EEG/-fMRI analysis approach to explore resting-state networks. *NeuroImage*, *52*, 1149–1161. http://doi.org/10.1016/j.neuroimage.2010.01.093

Newberg, A., Alavi, A., & Reivich, M. (2002). Determination of regional cerebral function with FDG-PET imaging in neuropsychiatric disorders. *Seminars in Nuclear Medicine*, *32*(1), 13–34. http://doi.org/10.1053/snuc.2002.29276

Newberg, A., Monti, D., Moss, A., & Alavi, A. (2012). Positron emission tomography in neurological and psychiatric disorders. *International Journal of Imaging Systems and Technology*, *22*(1), 2–17. http://doi.org/10.1002/ima.22004

Niazy, R. K., Beckmann, C. F., Iannetti, G. D., Brady, J. M., & Smith, S. M. (2005). Removal of FMRI environment artifacts from EEG data using optimal basis sets. *NeuroImage*, *28*(3), 720–737. http://doi.org/10.1016/j.neuroimage.2005.06.067

Nishida, K., Morishima, Y., Yoshimura, M., Isotani, T., Irisawa, S., Jann, K., … Koenig, T. (2013). EEG microstates associated with salience and frontoparietal networks in frontotemporal dementia, schizophrenia and Alzheimer's disease. *Clinical Neurophysiology*, *124*(6), 1106–1114. http://doi.org/10.1016/j.clinph.2013.01.005

Nishida, M., Asano, E., Juhász, C., Muzik, O., Sood, S., & Chugani, H. T. (2008). Cortical glucose metabolism correlates negatively with delta-slowing and spike-frequency in epilepsy associated with tuberous sclerosis. *Human Brain Mapping*, *29*(11), 1255–1264. http://doi.org/10.1002/hbm.20461

Oakes, T. R., Pizzagalli, D. A., Hendrick, A. M., Horras, K. A., Larson, C. L., Abercrombie, H. C., … Davidson, R. J. (2004). Functional coupling of simultaneous electrical and metabolic activity in the human brain. *Human Brain Mapping*, *21*(4), 257–270. http://doi.org/10.1002/hbm.20004

Ogawa, S., Lee, T. M., Kay, A. R., & Tank, D. W. (1990). Brain magnetic resonance imaging with contrast dependent on blood oxygenation. *Biophysics*, *87*, 9868–9872.

O'Halloran, R., Kopell, B. H., Sprooten, E., Goodman, W. K., & Frangou, S. (2016). Multimodal neuroimaging-informed clinical applications in neuropsychiatric disorders. *Frontiers in Psychiatry*, *7*, 63. http://doi.org/10.3389/fpsyt.2016.00063

Polikar, R., Tilley, C., Hillis, B., & Clark, C. M. (2010). *Multimodal EEG, MRI and PET data fusion for Alzheimer's disease diagnosis*. 2010 Annual International Conference of the IEEE Engineering in Medicine and Biology Society, pp. 6058–6061, Aug 31–Sep 4 2010, Buenos Aires. http://doi.org/10.1109/IEMBS.2010.5627621

Raichle, M. E. (2015). The Brain's default mode network. *Annual Review of Neuroscience.*, *38*, 433–447. http://doi.org/10.1146/annurev-neuro-071013-014030

Raichle, M. E., & Snyder, A. Z. (2007). A default mode of brain function: A brief history of an evolving idea. *NeuroImage*, *37*, 1083–1090. http://doi.org/10.1016/j.neuroimage.2007.02.041

Rajkumar, R., Rota Kops, E., Mauler, J., Tellmann, L., Lerche, C., Herzog, H., et al. (2017) Simultaneous trimodal PET-MR-EEG imaging: Do EEG

caps generate artefacts in PET images? *PLoS ONE 12*(9), e0184743. https://doi.org/10.1371/journal.pone.0184743

Riedl, V., Bienkowska, K., Strobel, C., Tahmasian, M., Grimmer, T., Förster, S., … Drzezga, A. (2014). Local activity determines functional connectivity in the resting human brain: A simultaneous FDG-PET/fMRI study. *The Journal of Neuroscience*, *34*(18), 6260–6266. http://doi.org/10.1523/JNEUROSCI.0492-14.2014

Riedl, V., Utz, L., Castrillón, G., Grimmer, T., Rauschecker, J. P., Ploner, M., … Sorg, C. (2015). Metabolic connectivity mapping reveals effective connectivity in the resting human brain. *Proceedings of the National Academy of Sciences of the United States of America*, *113*(2), 201513752. http://doi.org/10.1073/pnas.1513752113

Ritter, P., & Villringer, A. (2006). Simultaneous EEG-fMRI. *Neuroscience and Biobehavioral Reviews*, *30*(6), 823–838. http://doi.org/10.1016/j.neubiorev.2006.06.008

Rota Kops, E., Hautzel, H., Herzog, H., Antoch, G., & Shah, N. J. (2015). Comparison template-based versus CT-based attenuation correction for hybrid MR/PET scanners. *IEEE Transactions on Nuclear Science*, *62*(5), 2115–2121. http://doi.org/10.1109/TNS.2015.2452574

Seethalakshmi, R., Parkar, S. R., Nair, N., Adarkar, S. A., Pandit, A. G., Batra, S. A., … Moghe, S. H. (2006). Regional brain metabolism in schizophrenia: An FDG-PET study. *Indian Journal of Psychiatry*, *48*(3), 149–153. http://doi.org/10.4103/0019-5545.31577

Seitzman, B. A., Abell, M., Bartley, S. C., Erickson, M. A., Bolbecker, A. R., & Hetrick, W. P. (2017). Cognitive manipulation of brain electric microstates. *NeuroImage*, *146*, 533–543. http://doi.org/https://doi.org/10.1016/j.neuroimage.2016.10.002

Shah, N. J., Arrubla, J., Rajkumar, R., Farrher, E., Mauler, J., Rota Kops, E., … Neuner, I. (2017). Multimodal fingerprints of resting state networks as assessed by simultaneous Trimodal MR-PET-EEG imaging. *Scientific Reports*, *7*(1), 6452. http://doi.org/10.1038/s41598-017-05484-w

Shah, N. J., Oros-Peusquens, A.-M. M., Arrubla, J., Zhang, K., Warbrick, T., Mauler, J., … Neuner, I. (2013). Advances in multimodal neuroimaging: Hybrid MR-PET and MR-PET-EEG at 3 T and 9.4 T. *Journal of Magnetic Resonance*, *229*, 101–115. http://doi.org/10.1016/j.jmr.2012.11.027

Shehzad, Z., Kelly, A. M. C., Reiss, P. T., Gee, D. G., Gotimer, K., Uddin, L. Q., … Milham, M. P. (2009). The resting brain: Unconstrained yet reliable. *Cerebral Cortex*, *19*(10), 2209–2229. http://doi.org/10.1093/cercor/bhn256

Shirer, W. R., Ryali, S., Rykhlevskaia, E., Menon, V., & Greicius, M. D. (2012). Decoding subject-driven cognitive states with whole-brain connectivity patterns. *Cerebral Cortex*, *22*(1), 158–165. http://doi.org/10.1093/cercor/bhr099

Shivamurthy, V. K. N., Tahari, A. K., Marcus, C., & Subramaniam, R. M. (2015). Brain FDG PET and the diagnosis of dementia. *AJR. American Journal of Roentgenology*, *204*, W76–W85. http://doi.org/10.2214/AJR.13.12363

Simon, R., & Engström, M. (2015). The default mode network as a biomarker for monitoring the therapeutic effects of meditation. *Frontiers in Psychology*, *06*, 776. http://doi.org/10.3389/fpsyg.2015.00776

Skåtun, K. C., Kaufmann, T., Tønnesen, S., Biele, G., Melle, I., Agartz, I., … Westlye, L. T. (2016). Global brain connectivity alterations in patients with schizophrenia and bipolar spectrum disorders. *Journal of Psychiatry & Neuroscience*, *41*(3), 150159. http://doi.org/10.1503/jpn.150159

Sokoloff, L. (1981). Relationships among local functional activity, energy metabolism, and blood flow in the central nervous system. *Federation Proceedings*, *40*(8), 2311–2316.

Stevens, A., Günther, W., Lutzenberger, W., Bartels, M., & Müller, N. (1996). Abnormal topography of EEG microstates in Gilles de la Tourette syndrome. *European Archives of Psychiatry and Clinical Neuroscience*, *246*(6), 310–316. http://doi.org/10.1007/BF02189024

Stevens, A., Lutzenberger, W., Bartels, D. M., Strik, W., & Lindner, K. (1997). Increased duration and altered topography of EEG microstates during cognitive tasks in chronic schizophrenia. *Psychiatry Research*, *66*(1), 45–57. http://doi.org/10.1016/S0165-1781(96)02938-1

Stuart, A. (1956). Rank correlation methods. In M. G. Kendall (Ed.), 2nd ed. British journal of statistical psychology, 9(1).

Thie, J. A. (2004). Understanding the standardized uptake value, its methods, and implications for usage. *The Journal of Nuclear Medicine*, *45*(9), 1431–1434 Retrieved from http://www.ncbi.nlm.nih.gov/pubmed/15347707

Tibshirani, R., & Walther, G. (2005). Cluster validation by prediction strength. *Journal of Computational and Graphical Statistics*, *14*(3), 511–528 http://doi.org/10.1198/106186005X59243

Tomasi, D., & Volkow, N. D. (2012). Aging and functional brain networks. *Molecular Psychiatry*, *17*(5), 549–558 http://doi.org/10.1038/mp.2011.81

Tomasi, D., Wang, G.-J., & Volkow, N. D. (2013). Energetic cost of brain functional connectivity. *PNAS*, *110*(33), 13642–13647 http://doi.org/10.1073/pnas.1303346110

Tomescu, M. I., Rihs, T. A., Becker, R., Britz, J., Custo, A., Grouiller, F., … Michel, C. M. (2014). Deviant dynamics of EEG resting state pattern in 22q11.2 deletion syndrome adolescents: A vulnerability marker of schizophrenia? *Schizophrenia Research*, *157*(1–3), 175–181. http://doi.org/10.1016/j.schres.2014.05.036

Uludağ, K., & Roebroeck, A. (2014). General overview on the merits of multimodal neuroimaging data fusion. *NeuroImage*, *102*, 3–10. http://doi.org/10.1016/j.neuroimage.2014.05.018

Van De Ville, D., Britz, J., Michel, C. M., & Nikos Logothetis, K. (2010). EEG microstate sequences in healthy humans at rest reveal scale-free dynamics. *PNAS*, *107*(42), 18179–18184 http://doi.org/10.1073/pnas.1007841107

Winkler, I., Haufe, S., & Tangermann, M. (2011). Automatic classification of artifactual ICA-components for artifact removal in EEG signals. *Behavioral and Brain Functions*, *7*(30), 1–15. http://doi.org/10.1186/1744-9081-7-30

Xi, Q., Zhao, X., Wang, P., Guo, Q., Jiang, H., Cao, X., … Yan, C. (2012). Spontaneous brain activity in mild cognitive impairment revealed by amplitude of low-frequency fluctuation analysis: A resting-state fMRI study. *Radiologia Medica*, *117*(5), 865–871. http://doi.org/10.1007/s11547-011-0780-8

Yan, C. G., Di Wang, X., Zuo, X. N., & Zang, Y. F. (2016). DPABI: Data processing & analysis for (resting-state) brain imaging. *Neuroinformatics*, *14*(3), 339–351. http://doi.org/10.1007/s12021-016-9299-4

Yao, N., Shek-Kwan Chang, R., Cheung, C., Pang, S., Lau, K. K., Suckling, J., … Mcalonan, G. M. (2014). The default mode network is disrupted in Parkinson's disease with visual hallucinations. *Human Brain Mapping*, *35*, 5658–5666. http://doi.org/10.1002/hbm.22577

Yuan, H., Zotev, V., Phillips, R., Drevets, W. C., & Bodurka, J. (2012). Spatiotemporal dynamics of the brain at rest - Exploring EEG microstates as electrophysiological signatures of BOLD resting state networks. *NeuroImage*, *60*(4), 2062–2072. http://doi.org/10.1016/j.neuroimage.2012.02.031

Zang, Y., He, Y., Zhu, C., Cao, Q., Sui, M., Liang, M., … Wang, Y. (2007). Altered baseline brain activity in children with ADHD revealed by resting-state functional MRI. *Brain & Development*, *29*(2), 83–91. http://doi.org/10.1016/j.braindev.2006.07.002

Zang, Y., Jiang, T., Lu, Y., He, Y., & Tian, L. (2004). Regional homogeneity approach to fMRI data analysis. *NeuroImage*, *22*, 394–400. http://doi.org/10.1016/j.neuroimage.2003.12.030

Zhang, Y., Han, J., Hu, X., Guo, L., & Liu, T. (2013). *Data-driven evaluation of functional connectivity metrics.* In Proceedings - 2013 I.E. 10th International Symposium on Biomedical Imaging, pp. 532–535, San Fransciso, CA. http://doi.org/10.1109/ISBI.2013.6556529

Zhou, L., Pu, W., Wang, J., Liu, H., Wu, G., Liu, C., … Liu, Z. (2016). Inefficient DMN suppression in schizophrenia patients with impaired cognitive function but not patients with preserved cognitive function. *Scientific Reports*, *6*, 21657. http://doi.org/10.1038/srep21657

Zou, Q. H., Zhu, C. Z., Yang, Y., Zuo, X. N., Long, X. Y., Cao, Q. J., … Zang, Y. F. (2008). An improved approach to detection of amplitude of low-frequency fluctuation (ALFF) for resting-state fMRI: Fractional ALFF. *Journal of Neuroscience Methods*, *172*(1), 137–141. http://doi.org/10.1016/j.jneumeth.2008.04.012

Zuo, X. N., Di Martino, A., Kelly, C., Shehzad, Z. E., Gee, D. G., Klein, D. F., … Milham, M. P. (2010). The oscillating brain: Complex and reliable. *NeuroImage*, *49*(2), 1432–1445. http://doi.org/10.1016/j.neuroimage.2009.09.037

Zuo, X. N., Ehmke, R., Mennes, M., Imperati, D., Castellanos, F. X., Sporns, O., & Milham, M. P. (2012). Network centrality in the human functional connectome. *Cerebral Cortex*, *22*(8), 1862–1875. http://doi.org/10.1093/cercor/bhr269

Zuo, X. N., Xu, T., Jiang, L., Yang, Z., Cao, X. Y., He, Y., … Milham, M. P. (2013). Toward reliable characterization of functional homogeneity in

the human brain: Preprocessing, scan duration, imaging resolution and computational space. *NeuroImage*, *65*, 374–386. http://doi.org/10.1016/j.neuroimage.2012.10.017

SUPPORTING INFORMATION

Additional supporting information may be found online in the Supporting Information section at the end of the article.

How to cite this article: Rajkumar R, Farrher E, Mauler J, et al. Comparison of EEG microstates with resting state fMRI and FDG-PET measures in the default mode network via simultaneously recorded trimodal (PET/MR/EEG) data. *Hum Brain Mapp*. 2021;42:4122–4133. https://doi.org/10.1002/hbm.24429